

Feasibility study on ground-state cooling and single-phonon readout of trapped electrons using hybrid quantum systems

Alto Osada,^{1,2,*} Kento Taniguchi,¹ Masato Shigefuji,¹ and Atsushi Noguchi^{1,3,4,†}

¹*Komaba Institute for Science (KIS), The University of Tokyo, Meguro-ku, Tokyo, 153-8902, Japan*

²*PRESTO, Japan Science and Technology Agency, Kawaguchi-shi, Saitama 332-0012, Japan*

³*RIKEN Center for Quantum Computing (RQC), RIKEN, Wako-shi, Saitama 351-0198, Japan*

⁴*Inamori Research Institute for Science (InaRIS), Kyoto-shi, Kyoto, 600-8411, Japan*

(Dated: August 17, 2022)

Qubits of long coherence time and fast quantum operations are long-sought objectives towards the realization of high-fidelity quantum operations and their applications to the quantum technologies. An electron levitated in a vacuum by a Paul trap is expected to be a good candidate, for its light mass and hence the high secular frequency which allows for the faster gate operations than those in trapped ions. Controlling the motional state of the trapped electron is a crucial issue, for it mediates an interaction between electron spins, intrinsic qubits embedded in electrons, and its decoherence results in degraded fidelity of two-qubit gates. In addition, an efficient readout of the motional state is important, regarding the possibility of detecting spin state by using it. Despite of such an importance, how to achieve the motional ground state and how to efficiently detect it are not reported so far. Here we propose methods addressing these issues by utilizing hybrid quantum systems involving electron-superconducting circuit and electron-ion coupled systems and analyze the feasibility of our schemes. In both systems, we show that the ground-state cooling and the single-phonon readout of the motional state of the trapped electron are possible. Our work shed light on the way to precisely control the motional states of the trapped electrons, that provides an interesting playground for the development of quantum technologies.

I. INTRODUCTION

In recent development of quantum technologies, quantum bits (qubits) with long coherence times are explored in various platforms such as trapped ions [1], Rydberg atoms [2], superconducting circuits [3], and quantum defects in solids [4]. For instance, hyperfine and optical qubits in atomic ions in a Paul trap possess long coherence times thanks to their intrinsic nature being protected by levitating them in ultrahigh-vacuum environment [1]. As another example, lifetimes of the superconducting qubits have improved by several orders of magnitude [3] for a few decades. For characterizing how good the coherence times are for various qubits, a ratio ϵ of

the coherence time to the longest duration of quantum operation is useful, for its inverse limits the minimum-achievable error rates. In terms of this index, $\epsilon \sim 10^5$ and $\epsilon \sim 10^3$ are realized so far in hyperfine qubit of atomic ions [5] and superconducting qubits [6], respectively. To further develop error-corrected qubits by e.g., using a surface code [7, 8], a large number of physical qubits should form a single logical qubit. In this regard, it is highly demanded to achieve higher value of ϵ since it is beneficial for achieving higher fidelities and thus for reducing the required number of physical qubits for a single logical qubit.

For such a purpose, trapped-electron system [9–13] is a good candidate. An electron is a spin-1/2 system, literally being a pure two-level system or an intrinsic qubit without any other internal states into which the quantum information leaks. Likewise in the trapped-ion electron-spin qubit [14], the levitated electron-spin qubit is expected to maintain its coherence for orders-of-magnitude longer time compared to the solid-state counterparts [see e.g., Ref. [15] and references therein]. Trapped electrons also exhibit phonon degrees of freedom as trapped ions do, in which the phonon can be used as a quantum bus to implement a two-qubit gate [16] and can be utilized for detecting the spin state [17]. It is noteworthy that owing to more than 10 000 times lighter mass of an electron than those of ions, frequency of the phonon mode can be made as high as several hundreds of MHz or even be designed in the GHz region. Therefore, two-qubit gates in the trapped electron system are expected to be implemented within tens of nanoseconds when limited by the oscillation period of the electron. On top of that, zero-point fluctuation x_{zpf} of the phonon reaches 100 nm

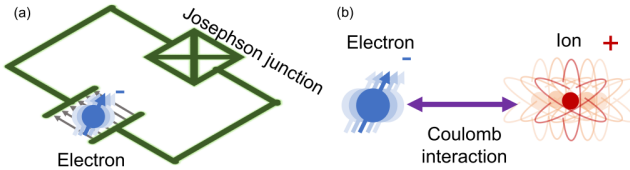


FIG. 1. Schematic illustrations of hybrid quantum systems considered in this work. (a) Coupled electron-superconducting qubit system where oscillatory electric field of a capacitor provides the coupling between an electron and a superconducting qubit. (b) Coupled trapped electron-trapped ion system with Coulomb attraction.

* alto@g.ecc.u-tokyo.ac.jp

† u-atsushi@g.ecc.u-tokyo.ac.jp

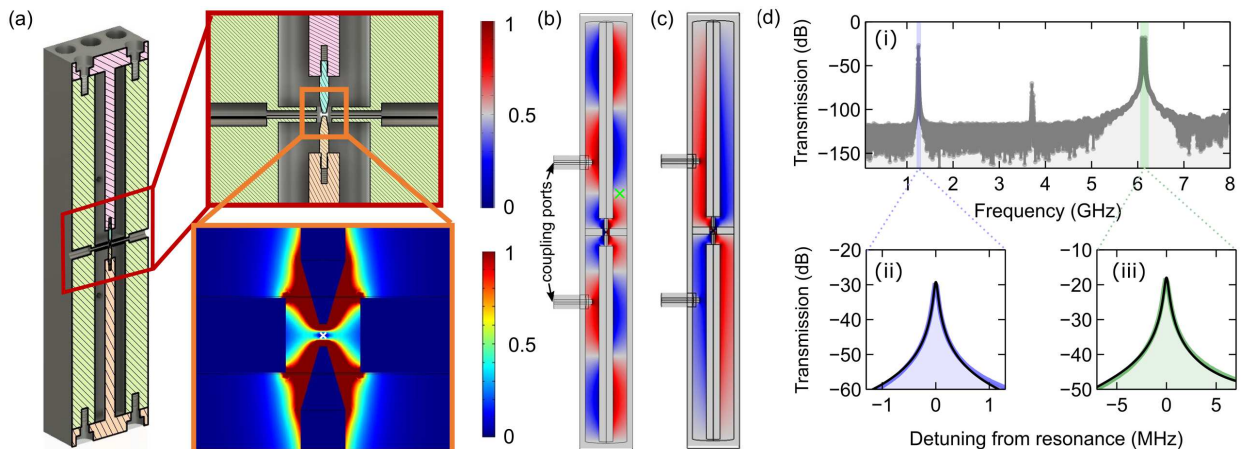


FIG. 2. Microwave-trap design and its characterization. (a) Cross-sectional view of the coupled coaxial cavity. Insets show the expanded view and the normalized pseudo-potential for an electron with colorscale given in the right panel of (c). (b) Field profiles of $5\lambda/4$ mode, or trap mode, used for the formation of pseudo-potential. Green cross schematically indicates a node of the mode where a transmon qubit is placed, see Sec. II C 2. (c) That of $\lambda/4$ mode, or the readout mode, utilized for the motional-state readout. (d) Observed transmission spectra of the coupled coaxial cavity by two-port measurement, with expanded plots of the trap mode (indicated by green) and the readout mode (indicated by blue). The black solid curves are Lorentzian fittings. Each mode exhibits, indeed, two peaks corresponding to symmetric and anti-symmetric modes. The expanded plots display the anti-symmetric $\lambda/4$ - and symmetric $5\lambda/4$ modes under concern.

range, 10 times greater than the ions'. The larger the zero-point fluctuation is, the stronger the interaction to the other systems exhibiting electromagnetic waves. In short, trapped electrons potentially possess longer coherence time than superconducting qubits and shorter gate duration than trapped ions, and thus are promising building blocks of the quantum technologies.

Electrons in a Paul trap have just been realized recently [12], and high-fidelity quantum operations [13], spin-state detection [17] and coupling to superconducting electronics for the quantum-state conversion [10] are discussed. A few more things should be addressed in order to fully utilize above advantages. First thing is a highly sensitive readout of the motional state of a single trapped electron. The readout of motional state, in particular, is of great interest in the scope of phonon-mediated spin-state readout as discussed in Ref. [17]. Second, electrons' motion has to be cooled down close to its vibrational ground state to eliminate the gate errors. Resistive cooling [9, 18] at low temperature will help electrons to get sympathetically cooled with the trapping electrodes, that said, active methods of cooling electrons are preferable since such cooling process does not afford the ground-state cooling at 4 K. We would like to mention that a levitated electron does not have any optical transitions, that hinders the straightforward application to quantum network [19]. Therefore, the connectivity of an electron to an optical photon is also a major concern.

In this article, we propose several methods that potentially resolve above issues by considering hybrid quantum systems comprised of trapped electrons, superconducting circuits and trapped ions, where electric fields of a superconducting circuit and a trapped ion can be uti-

lized as sources of interaction (see Fig. 1). By utilizing such quantum systems, we reveal that the single-phonon readout and ground-state cooling of the motional state of electrons, and that the quantum operations are feasible not only by radio-frequency or microwave fields but also by optical means, nevertheless a trapped-electron does not have optical transition. We also experimentally implement a few essential tools indispensable for realizing the ideas including a superconducting resonator and a cryocooler-compatible, low-energy electron source. Our results add fundamental building blocks for a growing field of trapped electron and pave the way for realizing an electron-based quantum computation.

This article is constructed as follows. In Sec. II, we first introduce a coupled coaxial cavity for trapping electrons and for reading out the motional state of the trapped electron, using resonant modes held in the cavity. Further using a dispersively-coupled cavity-transmon system, the electron's motion can be cooled down to its ground state and read out at the single-phonon level. Then we switch the topic to the electron-ion coupled system in Sec. III. Simultaneous Paul trapping of electrons and ions is proposed first and their coupling through the Coulomb attraction is discussed. Single-phonon readout and ground-state cooling for the trapped electron is shown to be feasible with the trapped ion as well. Sec. IV summarizes the results.

II. TRAPPED ELECTRON AND SUPERCONDUCTING CIRCUIT

A. Coaxial-cavity trap

By combining static and oscillatory quadrupolar electric fields, the Paul trap provides a powerful tool to trap charged particles, which has become a core technology in trapped-ion-based quantum computing [1] and quantum metrology [20]. Electrons trapped in a Paul trap exhibit the secular oscillation at the frequency of the order of GHz [13], which can be resonantly coupled to electromagnetic fields of the ultralow-loss superconducting circuits. Superconducting coaxial cavity is utilized for cavity quantum electrodynamics (QED) and microwave quantum optics (see e.g. Ref. [21] and references therein) for its high quality factor and large field concentration. We adopt it for the electron trapping as well, as detailed below.

Figure 2(a) schematically shows a coaxial-cavity based electron Paul trap investigated in this work. Two coaxial cavities, each consisting of a coaxial line terminated at a tip, are opposed to each other. Since each coaxial cavity forms a $\lambda/4$ resonator with grounded and floated edges, it supports a fundamental $\lambda/4$ mode and a series of higher-order modes with wavelengths assigned by $(2n + 1)\lambda/4$ with n being a positive integer. The electrode tips with $400\ \mu\text{m}$ -diameter circular apices are placed $400\ \mu\text{m}$ apart from each other, which yield the distance between the effective-potential minimum and the electrode tip r_0 to be $200\ \mu\text{m}$. The upper and lower coaxial cavities couple to each other capacitively by the electrode tips to result in the appearance of hybridized modes with symmetric and anti-symmetric electric-field distributions. The symmetric mode exhibits a quadrupolar electric field between the electrode tips to form an effective potential for the electron. The effective-potential landscape is shown in the right-bottom inset of Fig. 2(a) which is obtained by numerical method using COMSOL. The whole electric-field distribution of the symmetric $5\lambda/4$ resonance, which is called trap mode here, is shown in Fig. 2(b) as well. The simulated trap mode possesses the resonant frequency of 6.0 GHz. By assuming that its quality factor amounts 10^6 [21], the effective potential yields 3.0 eV depth and the secular frequency of 1.2 GHz with 0.8 mW input.

In contrast, the anti-symmetric mode generates a dipolar field at the effective-potential minimum. This can be utilized for a coupling to a secular motion of electrons and allows us for cavity-assisted electrical detection of them, as will be discussed further in Sec. II C. We utilize an anti-symmetric $\lambda/4$ resonance, which we call readout mode, of the same coupled coaxial cavity for this purpose, since it exhibits the resonance frequency of 1.2 GHz that is resonant on the secular motion of the electrons in the design described above. The electric-field distribution of the readout mode is displayed in Fig. 2(c).

In order to investigate the realizability of above trap

design, we constructed and evaluated the coupled coaxial cavity made of aluminum in practice under 300 mK environment realized by a ^3He -based cryocooler. We implement two-port measurements through two coupling ports attached symmetrically to the two coaxial cavities. The transmission spectra are shown in Fig. 2(d). In the spectrum Fig. 2(d-i), three peaks at 1.2 GHz, 3.7 GHz and 6.1 GHz correspond respectively to $\lambda/4$, $3\lambda/4$ and $5\lambda/4$ resonances. The spectra of readout and trap modes are plotted in Fig. 2(d-ii) and (d-iii), respectively. Black curves are Lorentzian fittings that yield the intrinsic quality factor of 1.8×10^4 for the readout mode and a similar value is obtained for the trap mode. Even with this quality factor of the trap mode being lower than the assumed value of 10^6 in the numerical estimation, 2 mW injection is estimated to give the same effective potential for the electrons if we use optimized, sharper electrode tips, without spoiling the cryogenic environments.

B. Cryocooler-compatible low-energy electron source

In the recent room-temperature implementation of Paul trapping of electrons [12], neutral atoms from an oven are photoionized to realize the *in situ* generation of electrons of sufficiently low energy for the trapping. However, cryogenic environment does not afford devices with large heat production exceeding the cooling power. Therefore, the use of oven is hindered and an alternative method is required. In such a perspective, pulsed laser ablation [22–25] for the generation of neutral atoms is widely recognized as a cryocooler-compatible method, for it utilizes short-term, local heating of the target material to generate a tiny jet of atom flux.

Such a method is directly applicable to the electron generation that is naturally involved in the photoionization of neutral atoms. Figure 3(a) shows a schematics of a proposed low-energy electron source. A pulsed nanosecond 1064 nm-wavelength laser impinges on an ablation target to generate a neutral atoms to be photoionized. For instance, calcium atoms are ablated out of the calcium titanate (CaTiO_3), which is revealed to be a long-lived calcium atom source enduring over thousands of ablation pulses (see Appendix A). A jet of calcium atoms is then introduced into the trapping region of the coupled coaxial cavity. Other two lasers also points toward the trapping region to photoionize the atoms, by driving optical transitions of calcium atom with transition wavelengths 423 nm ($^1S_0 \rightarrow ^1P_1$) and 390 nm (from 1P_1 to continuum) [12, 26]. Generated electron carries excess energy brought by the second laser, or more concretely, the energy difference $E_L - E_{\text{th}}$ of the incident 390 nm-wavelength photon E_L and the ionization-threshold energy E_{th} from 1P_1 state, that corresponds to the wavelength of 389.81 nm [26], can naively be regarded as the energy of the generated electrons. Therefore, the energy of the electron can be tuned by E_L in this scheme. In

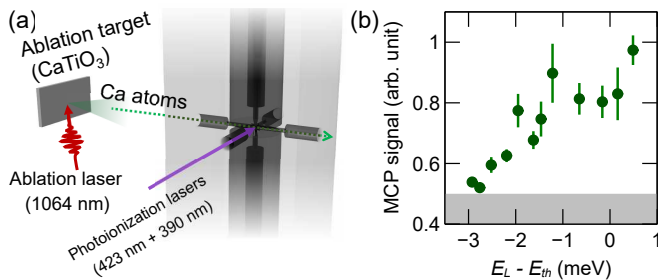


FIG. 3. Cryocooler-compatible electron generation. (a) Proposed experimental system of the electron generation based on Ca atom generation by 1064 nm-wavelength nanosecond pulsed-laser ablation and succeeded photoionization. In experiment (b), a multi-channel plate (MCP) is placed instead of the coupled coaxial cavity. (b) Signal of electrons detected by an MCP. The electrons are generated by the combination of pulsed-laser ablation and photoionization as depicted in (a). Horizontal axis represents the energy of the 390 nm-wavelength ionization laser, relative to the E_{th} . The upper bound of the gray shaded region stands for the background signal level, namely the MCP signal without the 423 nm-wavelength photoionization laser. Error bars represent one standard deviation.

addition, the electron generation process is comprised of the laser ablation and the photoionization, so that this all-optical method can be done in a pulsed manner, resulting in negligible heat production and hence compatibility with a cryogenic environment.

To demonstrate our electron generation scheme, we placed a CaTiO_3 as an ablation target and a multi-channel plate (MCP) with electrodes for guiding and accelerating electrons in a vacuum chamber at room temperature. In this experiment we do not have coupled coaxial cavity in the ionization region. The laser pulse for ablation is applied with its single-pulse energy of $76 \mu\text{J}$ and corresponding pulse fluence of 1 J/cm^2 . When the repetition rate of the pulse is 1 Hz, this pulse irradiation results in only $76 \mu\text{W}$ heat generation if all the energy was absorbed by the sample. Such an experimental condition allows us to observe sizable signals of electrons at MCP. In Fig. 3(b), MCP signal, which is proportional to a number of generated electrons, is plotted for various energies E_L of the photoionization laser around the ionization threshold E_{th} . As E_L approaches and exceeds E_{th} , a bright spot indicating the detection of electrons appears on the phosphor screen of the MCP. This signals the successful generation of electrons by the combination of laser ablation and succeeding photoionization of calcium atoms. We could also demonstrate the compatibility of this method with a ^3He -based cryocooler with a separate experiment.

Considering that the energy difference $E_L - E_{\text{th}}$ corresponds to the energy of the electron, successfully generated electrons in Fig. 3(b) are deduced to have their kinetic energy of less than several meV, which is much smaller than the depth of the effective potential.

C. Readout of motional state

1. Electrical readout

As mentioned in Sec. II A, we utilize the anti-symmetric $\lambda/4$ mode of the coupled coaxial cavity for the readout of the secular motion of trapped electrons. The predominant interaction between microwave field and such phonon mode of an electron, which we call it simply the phonon hereafter, is electric dipole interaction. Let the phonon mode and the readout mode respectively have their eigenfrequencies ω_e and ω_{MW} , with their respective annihilation operators \hat{a} and \hat{b} . The phonon-cavity interaction described above leads to a total Hamiltonian \hat{H}_{ec} of such a hybrid system written as

$$\hat{H}_{\text{ec}} = \hbar\omega_e \hat{a}^\dagger \hat{a} + \hbar\omega_{\text{MW}} \hat{b}^\dagger \hat{b} + \hbar g_{\text{ec}} (\hat{a}^\dagger \hat{b} + \hat{a} \hat{b}^\dagger) \quad (1)$$

where the phonon-cavity interaction is incorporated in the third term under the rotating-wave approximation. The coupling strength reads $g_{\text{ec}} = ex_{\text{zpf}} E_{\text{zpf}}$ with $x_{\text{zpf}} = \sqrt{\hbar/2m_e\omega_e}$ representing zero-point fluctuation of the phonon mode and E_{zpf} being that of the electric field of the readout mode, respectively. The latter one, E_{zpf} , depends on the circuit design and numerical simulation using COMSOL reveals that $g_{\text{ec}}/2\pi = 33 \text{ kHz}$ in our coupled coaxial-cavity design.

The hybrid system then manifest itself as being in a strong coupling regime with such a coupling strength, by assuming that an intrinsic quality factor of more than 100 000 can be achieved for the readout mode. We can utilize this hybrid system for reading out the phonon state, by extracting microwaves radiated from the electron through the microwave cavity. The extraction will be efficient owing to the strong phonon-cavity coupling mentioned above and properly tuned external coupling of the cavity. With the use of a commercial high-electron-mobility-transistor amplifier, the sensitivity for the oscillatory motion of an electron can be estimated to be -195 dBm/Hz , corresponding to that of a few tens of phonons with unity signal-to-noise ratio.

2. Quantum non-demolition measurement using a Josephson circuit

As stated above, the phonon state can be read out resonantly through the superconducting microwave cavity, however, sensitivity is still insufficient for single-phonon detection. In addition, the coupling strength g_{ec} is not enough for phonon-number resolving measurement. With this observation, we are motivated to utilize another ingredient of a Josephson circuit, or more concretely a three-dimensional transmon qubit in our scheme. The transmon qubit has been placed inside the coupled coaxial cavity around the antinode of the cavity mode to implement cavity QED system in strong dispersive regime [27]. In our cavity design, the transmon qubit

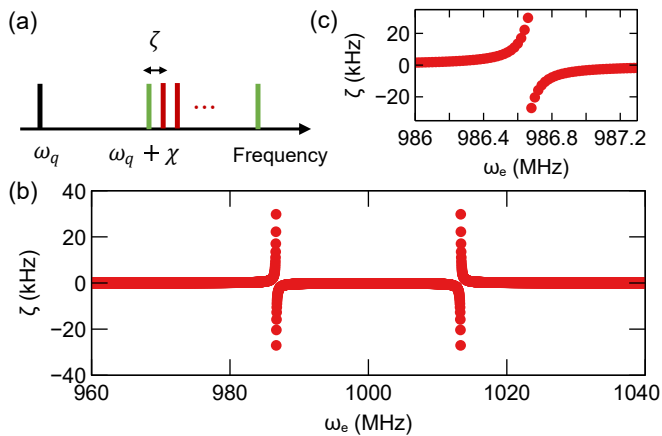


FIG. 4. Dispersive interaction of phonon of an electron and transmon qubit. (a) Schematic illustration of transmon-qubit spectrum with dispersive interactions. The original frequency of the transmon qubit (black) is predominately split into multiple copies (green) by the dispersive interaction with a microwave cavity mode, where the frequency spacing is approximately given by $\chi = g_{sc}^2/\Delta_{sc}$. Since the microwave cavity mode couples to the phonon mode of an electron, their spectra are dispersively shifted (indicated by red) as well, with the coupling strength ζ . (b) Numerically obtained values of ζ as a function of the phonon frequency ω_e . Detailed structure of the resonant behavior around $\omega_e/2\pi = 986$ MHz is shown in (c). Parameters used for this calculation are listed in Table. I.

should be put at the node of the trap mode [see Fig. 2(b)] so that it is unaffected by the presence of the transmon qubit. Transmon qubit at this position can still strongly couple to the readout mode. Let g_{sc} denote the coupling strength between the readout mode and the transmon qubit represented by Pauli operators. The Hamiltonian of the readout system now reads

$$\hat{H}'_{\text{read}} = \hat{H}'_{ec} + \hat{H}_{sc} \quad (2)$$

with $\hat{H}'_{ec} = \hbar\omega_e\hat{a}^\dagger\hat{a} + \hbar g_{ec}(\hat{a}^\dagger\hat{b} + \hat{a}\hat{b}^\dagger)$ and \hat{H}_{sc} defined by

$$\hat{H}_{sc} = \hbar\omega_{\text{MW}}\hat{b}^\dagger\hat{b} + \frac{\hbar\omega_q}{2}\hat{\sigma}_z + \hbar g_{sc}(\hat{b}^\dagger\hat{\sigma}_- + \hat{b}\hat{\sigma}_+). \quad (3)$$

Here ω_q is the transition frequency of the transmon qubit.

Suppose that the phonon frequency is resonant on the microwave cavity mode, while the transmon qubit is off-resonant. The coupled phonon-cavity system exhibits two normal modes, and the transmon qubit dispersively couples to the normal modes to experience a Stark effect in the presence of the phonon of the electron motion. Under a reasonable situation of $g_{ec} \ll g_{sc}$, we can first derive the dispersive Hamiltonian by applying Schrieffer-Wolff transformation [28] on \hat{H}_{sc} without the trapped-electron system and the coupling to it, yielding a dispersive Hamiltonian \hat{H}'_{sc} involving the readout mode and the transmon qubit [27] as

$$\hat{H}'_{sc} = \frac{\hbar}{2} \left(\omega_q + \frac{g_{sc}^2}{\Delta_{sc}} \right) \sigma_z + \hbar \left(\omega_{\text{MW}} + \frac{g_{sc}^2}{\Delta_{sc}} \sigma_z \right) b^\dagger b \quad (4)$$

with $\Delta_{sc} = \omega_{\text{MW}} - \omega_q$. Then by adding \hat{H}'_{ec} to it, further Schrieffer-Wolff transformation for $\hat{H}'_{sc} + \hat{H}'_{ec}$ brings the readout Hamiltonian into an approximately diagonalized form by regarding the off-diagonal term $\hbar g_{ec}(\hat{a}^\dagger\hat{b} + \hat{a}\hat{b}^\dagger)$ as a perturbation. The latter transformation is executed symbolically by Mathematica program. The resultant effective Hamiltonian contains the dispersive coupling between phonon mode and the transmon qubit $\hbar\zeta\hat{a}^\dagger\hat{a}\sigma_z$ with the coupling parameter ζ given by

$$\zeta = \frac{2g_{ec}^2g_{sc}^2\Delta_{sc}}{g_{sc}^4 - \Delta_{ec}^2\Delta_{sc}^2}. \quad (5)$$

Here the detuning $\Delta_{ec} = \omega_{\text{MW}} - \omega_e$ is introduced. Let us define here another detuning $\delta = \Delta_{ec} - g_{sc}^2/\Delta_{sc}$. This stands for the frequency difference between the phonon and the microwave cavity mode, where the latter one is now shifted due to the dispersive coupling to the transmon qubit. We can safely assume $|\delta| \ll |g_{sc}^2/\Delta_{sc}|$ to rewrite the above expression as

$$\zeta = -\frac{g_{ec}^2}{\delta}. \quad (6)$$

This is indeed a dispersive coupling between the phonon and the microwave cavity mode and is valid when $|\delta| \gg g_{ec}$. The coupling term $\hbar\zeta\hat{a}^\dagger\hat{a}\sigma_z$, after all, imprints the phonon-number-dependent spectrum of coupled phonon-cavity system onto the transmon spectrum [see Fig. 4(a)]. Even if $|\delta| \gg g_{ec}$ does not hold, i.e. the coupled phonon-cavity system is near resonant, $|\zeta| \simeq g_{ec}$ can be obtained at most. For comparison, we plot ζ with respect to ω_e obtained by numerical diagonalization of \hat{H}'_{read} in Fig. 4(b) and (c). The parameters used for this calculation are listed in Table. I.

In the strong dispersive regime in which ζ overwhelms decoherence rates of the phonon mode, readout mode and transmon qubit, the phonon number will be resolved, likewise in the circuit QED systems [29]. With the large quality factor $\sim 10^6$ of the cavity mode and the long coherence time $\sim 60 \mu\text{s}$ of the qubit [21], a phonon-number resolving experiment is feasible with a reasonable assumption that the coherence time of the phonon mode is as long as 10 ms.

D. Cooling with superconducting circuits

Phonon mode of trapped electrons can be used for implementing a two-qubit gate and its thermal excitation give rise to errors of the gate operations. Therefore, the

| | |
|---|---------|
| microwave-cavity-mode frequency, ω_{MW} | 1 GHz |
| transmon-qubit frequency, ω_q | 4 GHz |
| phonon-cavity coupling strength, g_{ec} | 33 kHz |
| qubit-cavity coupling strength, g_{sc} | 200 MHz |

TABLE I. Parameters used for the evaluation of ζ .

phonon is preferably prepared in its ground state, however, electrons do not possess internal structure except for the intrinsic spin degree of freedom, so that a powerful method of laser cooling, which enables us to obtain atomic ions in their motional ground state, is unavailable for the trapped-electron system. A trapped electron loses its motional energy predominantly through the resistive cooling [9, 18] that equilibrates the electron with thermal environment. At 300 mK environment with motional frequency of 1 GHz, mean phonon occupation number \bar{n} can be roughly estimated by assuming the Bose-Einstein distribution to be $\bar{n} \simeq 6$. Moreover, it is revealed that the heating rate for trapped electrons amounts 140 quanta per second [13], which may compete the resistive-cooling rate. Other ways than just using dilution refrigerator to cool the trapped electrons are highly demanded, and in this Section, we discuss two cooling methods: one using a cavity mode and another one using a transmon qubit and its measurement.

1. Cooling using a microwave cavity

A bottleneck of the resistive cooling is its cooling rate, that affords only partial cooling of electron's motion but not down close to its motional ground state, or even higher due to the competition with the heating rate. A straightforward idea of improving the cooling rate is to utilize a microwave resonator that is resonant with the phonon mode [11]. An oscillatory motion of an electron can couple to the readout mode and it allows for the coupling of phonon mode to the propagating mode with the rate ~ 33 kHz, as discussed in the previous Section. This cooling rate well surpasses the conservatively assessed heating rate of 140 Hz [13]. Thanks to this, the phonon mode equilibrates well with the thermal bath, which yields the mean phonon number of 6 at 300 mK environment.

2. Cooling using a transmon qubit

We have just considered the cooling of a phonon mode by the use of a coupling to the readout mode. Even with such a method, it allows the trapped electron to thermalize with the cryogenic environment, that is, the artificially added cooling and heating rates are relatively large but still totally equal. Further cooling beyond the temperature of the cryocooler ~ 300 mK is required for achieving the motional ground state.

Our approach is to utilize a circuit-QED system where a transmon qubit dispersively coupled to the readout mode. The coupling between them is typically in the MHz regime, which is much larger than g_{ec} , so that we can consider the circuit-QED system first and then take into account the trapped electron afterwards. We consider circuit-QED system and its quantum state $|\xi, n\rangle$ with the number of excitations n in the coupled coaxial

cavity and the qubit state $\xi = g, e$ or f respectively corresponding to the ground, first-excited or second-excited state. The cooling process we propose is as follows. First we consider the state $|g, 1\rangle$ and apply a π pulse of $|g, 1\rangle \leftrightarrow |f, 0\rangle$ transition to transfer the excitation from the cavity to the qubit, and consecutively apply a π pulse of $|e, 0\rangle \leftrightarrow |f, 0\rangle$ transition to bring the system in $|e, 0\rangle$ state. If we start with the $|g, 0\rangle$ state, above procedure does nothing. Finally the transmon qubit is read out through the $3\lambda/4$ mode of the coupled coaxial cavity, which we call the auxiliary mode. This procedure is a projective measurement thanks to the strong dispersive coupling between the auxiliary mode and the qubit, that transforms a mixed state to a pure state to reduce the entropy to result in the cooling down of the readout mode. At this point, let us recall that the electron is coupled to the readout mode. The electron therefore thermalizes with the readout mode and thus cooled down as well.

By adopting a similar scheme, using the decay of the transmon qubit rather than a measurement of it, mean photon number in a LC resonator with its resonant frequency being 173 MHz is cooled down to ~ 0.1 [30], corresponding to a mode temperature of 4 mK. Although this value is dependent on the temperature of the environment, the scheme itself is valid for the current setup as well. By applying a π -pulse which brings $|e, 0\rangle$ to $|g, 0\rangle$ instead of waiting for the qubit to decay, a single cooling cycle can be completed within $1.5 \mu\text{s}$, given that the Rabi frequency of the $|g, 1\rangle \leftrightarrow |f, 0\rangle$ and $|e, 0\rangle \leftrightarrow |f, 0\rangle$ transitions become a few MHz and that of $|g, 0\rangle \leftrightarrow |e, 0\rangle$ transition is on the order of 10 MHz, with the measurement time taking $\sim 1 \mu\text{s}$. The added cooling rate by above procedure thus amounts sub-MHz. This scheme, hence, is capable of reducing the mean photon number of the read mode down to its ground state and so for the motional state of the trapped electron. In this manner, the cooling using the transmon qubit and its measurement provides a way to achieve motional ground state of the trapped electron.

III. TRAPPED ELECTRON AND TRAPPED ION

In this Section, we introduce an electron-ion hybrid system in terms of the feasibility of simultaneous trapping of electrons and ions, state readout and cooling of the trapped electrons with the help of the ions.

A. Simultaneous trapping of electrons and ions

Electrons and ions interacts with each other by Coulomb interaction and thus the closer they are, the stronger the interaction becomes. Each of them can be trapped using a Paul trap, however, there are a few technical difficulties toward the simultaneous trapping of them. One is the large difference of their masses by a fac-

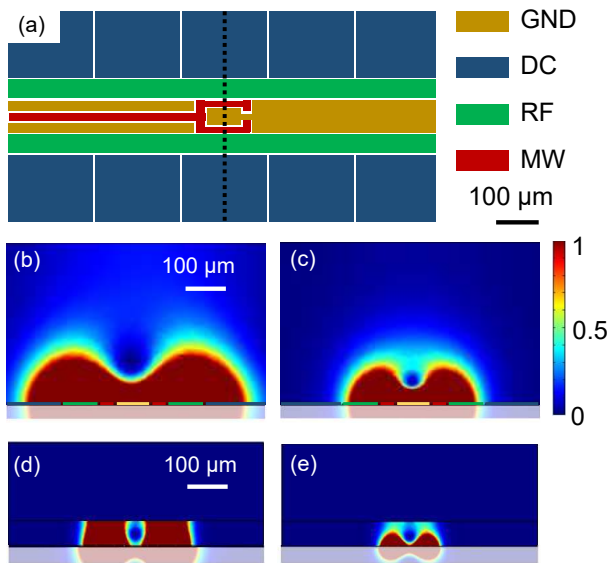


FIG. 5. Electrode design for simultaneous trapping of electrons and ions. (a) Surface-electrode configuration. Basic structure is a segmented five-rail linear Paul trap with a grounded electrode (GND, yellow) in the middle and RF electrodes (green) on the both sides of it. Confinement in the axial direction is realized by the segmented dc electrodes (blue). Grounded electrode is further divided and red part acts as a microwave electrode (MW), which can be regarded as a microwave ring trap and as a grounded one in the RF region. (b, c) Normalized pseudo-potential profiles for (b) an ion and (c) an electron in the cross-section along the black dotted line in (a). Scale bar is common for (b) and (c). (d, e) Normalized pseudo-potential profiles for (d) an ion and for (e) an electron with a grounded ceiling at $100 \mu\text{m}$ above the trap electrodes.

tor ranging from 10^4 to 10^5 . This results in a difference of the frequencies of their secular motions and those of supplied ac voltages to the trap, so that the design of the trap electrodes needs a special care [31–33]. Second issue is their signs of the charge. The atomic ions are positively charged and the electrons are, of course, negatively charged. The pseudo-potential formed by ac voltages are valid for both particles, but the linear Paul trap requires dc voltages as well and a simple end-cap structure does not provide axial trapping potential for both simultaneously. Additionally, it is desirable to have electrons and ions trapped close to each other, however, it is important to trap them separately with a finite distance, in order to avoid the trapping of electrons by atomic ions that give rise to recombination processes, that is rather of interest in a different context such as quantum chemistry realized in the single-particle level.

Our idea is to utilize a surface electrode trap with RF electrodes for trapping ions and microwave electrodes for electrons coexisting in-plane. A top view of the electrode design is schematically shown in Fig. 5(a). The electrode structure is a segmented five-rail linear Paul trap with grounded electrode (GND, yellow) in the middle and RF electrodes (green) on the both sides of it. Confinement in

the axial direction is realized by the segmented dc electrodes (blue). The grounded electrode is further divided and red part acts as a microwave electrode (MW), which can be regarded as a grounded one in the RF region and acts as a microwave ring trap for electrons. We set the widths of the GND and RF electrodes to be $160 \mu\text{m}$ and $80 \mu\text{m}$, respectively, and that of the MW electrodes at the cross-section to be $30 \mu\text{m}$.

As for an ion, on one hand, the trapping potential is nothing but a linear RF Paul trap, since the ion cannot follow the microwave field. On the other hand, an electron is trapped by a ring-like microwave Paul trap. Normalized pseudo-potential profiles for an ion and an electron in the cross-section along the black dotted line in Fig. 5(a) are respectively shown in Figs. 5(b) and (c). The trapping potential for an electron becomes 40 meV -depth and yields the secular frequency of 800 MHz with an applied 4 GHz -microwave voltage of 20 V . The trapping potential for an ion is estimated to be 20 meV -depth with secular frequency of 3 MHz by assuming the use of a beryllium ion and an application of 40 MHz -RF voltage of 30 V , which is sufficient for ion-trap experiments [34]. Here the grounded ceiling is located at $200 \mu\text{m}$ height.

Due to the slight difference of the electrode dimension, electrons and ions are trapped at different heights. The electrode design shown in Fig. 5(b,c) yields the difference of their heights by $50 \mu\text{m}$ and this difference can be made smaller down to $10 \mu\text{m}$ if we add a grounded ceiling plate at $100 \mu\text{m}$ above the trap to modify the pseudo-potential profiles, see Figs. 5(d) and (e). This situation, where the electrons and ions are trapped close but apart, is beneficial for preventing them from recombination while keeping sizable Coulomb interaction between them. The coupling between an electron and an ion simultaneously trapped with our proposed setup will be discussed in the following Sections.

B. Readout of motional state using trapped ions

As has been proposed in the previous Section, an electron and an ion can be trapped by applied ac voltages separately but close to each other. Here let us consider the interaction between them, starting from total potential energy U of the electron-ion hybrid system

$$U = \frac{1}{2}m_e\omega_e^2x^2 + \frac{1}{2}m_i\omega_i^2y^2 + V, \quad (7)$$

including the Coulomb energy

$$V = -\frac{e^2}{4\pi\epsilon_0} \frac{1}{L - y + x}. \quad (8)$$

In above expressions, an electron and an ion is trapped at positions separated by L and displacements from their trapping points are denoted as x for the electron and y for the ion. With subscripts e for the electron and i for the ion attached, m and ω represent the mass and secular frequency of each particle, respectively. Well-known

| $\omega_e/2\pi$ (MHz) | L (μm) | $g_0/2\pi$ (kHz) | $\alpha/2\pi$ (kHz) | \bar{n}_e |
|-----------------------|-----------------------|-------------------|---------------------|----------------------|
| 800 | 10 | 33 | -33 | 5.3×10^{-2} |
| 800 | 50 | 0.39 | -34 | 5.9 |
| 500 | 10 | 39 | -2.6×10^3 | 3.8×10^{-2} |
| 500 | 7 | 1.6×10^3 | -2.5×10^3 | 2.2×10^{-3} |

TABLE II. Coupling strengths of the electron-ion hybrid system for various parameters. g_0 : coupling strength of the optomechanical term, α : strength of the self-Kerr interaction, \bar{n}_e : estimated phonon number of a trapped electron. $\omega_i/2\pi = 2$ MHz is assumed in common.

physical constants of e , the elementary charge, and ϵ_0 , the vacuum permittivity, are also used.

Coulomb attraction V makes the electron and the ion bring themselves closer and the equilibrium points are shifted from the original trapping point. Moreover, the potential is distorted to get anharmonic since the Coulomb interaction is nonlinear by nature. We shall expand V under the assumption that the relative displacement is much smaller than the electron-ion distance, $|x - y| \ll L$. This expansion yields polynomials of x and y . The terms proportional to x and y result in the shift of positions and those to x^2 and y^2 lead to the shift of oscillation frequencies. The term xy contains a beam-splitter or two-mode-squeezing interactions. Higher-order terms x^3 , x^2y , xy^2 and y^3 stand for the second-order nonlinearities and x^4 , y^4 , ... represent the third-order nonlinearities. Since we consider the situation that the phonon frequencies of the electron and the ion are different, the beam-splitter and two-mode-squeezing interactions are not valid here. Likewise the rapidly oscillating terms are omitted and the series expansion is truncated in our analysis to get a Hamiltonian of the whole system as

$$\hat{H} = \hbar\omega_e\hat{a}^\dagger\hat{a} + \hbar\omega_i\hat{c}^\dagger\hat{c} - \hbar g_0\hat{a}^\dagger\hat{a}(\hat{c}^\dagger + \hat{c}) - \frac{\hbar\alpha}{2}\hat{a}^\dagger\hat{a}^\dagger\hat{a}\hat{a}, \quad (9)$$

where ω_e now stands for the renormalized secular frequency of a trapped electron and ω_i is the one for the trapped ion. The ladder operators of the phonon mode of the trapped ion are denoted by \hat{c} and \hat{c}^\dagger . The third term is much like an cavity optomechanical interaction, where the electron mimics the cavity and the ion plays the role of a mechanical oscillator. The coupling strength g_0 is given as

$$g_0 = \frac{1}{\hbar} \left(\frac{e^2}{4\pi\epsilon_0} \frac{6x_{\text{zpf}}^2 y_{\text{zpf}}}{L^4} - \frac{2\hbar g_C \beta}{\omega_e - \omega_i} \right) \quad (10)$$

using the zero-point fluctuations $x_{\text{zpf}} = \sqrt{\hbar/2m_e\omega_e}$ and $y_{\text{zpf}} = \sqrt{\hbar/2m_i\omega_i}$. In addition to the nonlinearity arising from the Coulomb interaction, we included the nonlinearity of electron motion arising from the effective potential itself in the second term. Along with this correction, we introduced $g_C = (1/\hbar)(\partial^2 V/\partial x \partial y)x_{\text{zpf}}y_{\text{zpf}}$. β is extracted from the second-order nonlinearity of the effective potential for the electron. Though the interaction

term is principally given by the optomechanical one, we include the fourth, self-Kerr term for it limits the driven number of phonons, as described in later paragraph. The constant α reads

$$\alpha = \alpha_C + \alpha_K - \frac{6\beta^2}{\omega_e} \quad (11)$$

where

$$\alpha_C = \frac{1}{\hbar} \frac{e^2}{4\pi\epsilon_0} \frac{12x_{\text{zpf}}^4}{L^5} \quad (12)$$

is the third-order nonlinearity and α_K the one from the effective potential for the electron. The Hamiltonian in Eq. (9) is obtained in the same manner as was done in Ref. [35].

Just as in the cavity optomechanics [36], the interaction term $\hbar g_0\hat{a}^\dagger\hat{a}(\hat{c}^\dagger + \hat{c})$ allows for the three-wave mixing, one of which is the phonon of an ion and two are the phonon of an electron. If we drive the electron motion with microwaves of its frequency being $\omega_e + \omega_i$, the linearized interaction appears as $\hbar g_0\sqrt{\bar{n}_d}(\hat{a}^\dagger\hat{c}^\dagger + \hat{a}\hat{c})$, with \bar{n}_d being the mean number of phonons of the electron. Driving field is assumed to be intense so that its amplitude can be thought of the mean phonon number of the driven mode. This two-mode-squeezing interaction amplifies the motion of the electron, whose state can be readout through a thermometry of the trapped ion.

The motion of the electron is driven in such a scheme, however, the self-Kerr term $(\hbar\alpha/2)\hat{a}^\dagger\hat{a}^\dagger\hat{a}\hat{a}$ imposes small but finite energy shift of the number states with large occupation numbers. This limits the mean number of phonons that can be excited by the drive tone, or in other words the effect of the driving saturates. The saturation occurs roughly when the frequency shift $\alpha\bar{n}_d$ gets comparable to the driving strength itself, $g = g_0\sqrt{\bar{n}_d}$. This tells us the limit of coupling strength g_{max} of g as

$$g_{\text{max}} = \frac{g_0^2}{\alpha}. \quad (13)$$

For various trapping parameters, we calculate the coupling strength g_0 and nonlinear coefficient α in Table II. In all these parameters, the driven oscillatory motion exhibits the oscillation amplitude of no more than a few micrometers, however, driven number of phonons is no more than 1 since g and α are comparable in their magnitudes. The motional state of the ion can be identified using its optical transition and even that of the electron is possible with this scheme.

C. Sympathetic cooling with trapped ion

When we drive the electron with $\omega_e - \omega_i$, the interaction term becomes $\hbar g(\hat{a}^\dagger\hat{c} + \hat{a}\hat{c}^\dagger)$. Suppose that the cooling rate of the ion's motion is Γ_i . Through the beam-splitter interaction synthesized above, the electron is sympathetically cooled [18] by a cooling rate of $\Gamma_\downarrow = 4g^2/\Gamma_i$, where

$\Gamma_i > g$ is assumed. Then the average phonon number of the electron is estimated by $\bar{n}_e = n_{\text{th}}\Gamma_{\text{th}}^e / (\Gamma_{\downarrow}^e + \Gamma_{\text{th}}^e)$, where $n_{\text{th}} = 12$ is the mean phonon number of the electron at 300 mK with the phonon frequency of 500 MHz and $\Gamma_{\text{th}}^e = \Gamma_{\text{th}}^e + \Gamma_i$ with Γ_{th}^e being the coupling rate of electron's motion to the thermal bath, which we shall conservatively assume it to be 10 Hz [13].

The values of g_{max} and the final occupation number \bar{n}_e are listed in Table. II for various parameters of the electron-ion coupled system with $\Gamma_i/2\pi = 10$ kHz being assumed as a typical value. The final occupation number \bar{n}_e can be well below unity by the thermalization with the ion in most conditions listed in the Table, which confirms the validity of sympathetic cooling of a trapped electron down to the motional ground state using a trapped ion. One concern is the possible heating of electrons (ions) due to the presence of the RF for trapping ions (electrons) in the two-frequency Paul trap, which should be investigated with the actual implementation of it in future work. One more thing that we would like to mention is that this method, the parametrically-driven sympathetic cooling of mass-imbalanced charged particles, is useful not only for the cooling of electrons but also in the ion-trap experiments, since our method allow us to avoid inefficiency of the sympathetic cooling of mass-imbalanced ions by bringing their motional frequency effectively on resonance.

IV. CONCLUSION

As a summary, we proposed and analyzed hybrid quantum systems consisting of a trapped electron interacting with superconducting circuits and a trapped ion. The basic idea of the electron trap using multiple modes of the $\lambda/4$ resonator and the cryocooler-compatible, low-energy electron source are introduced and proved to be valid for the use in proposed electron-trapping experiments. We further revealed that the light mass of the electron and hence the high secular-motion frequency of the trapped one result in the strong electron-circuit and electron-ion couplings, where the latter is aided by the nonlinearity of the Coulomb interaction. In both hybrid quantum systems, the single-phonon-level readout and the ground-state cooling of the motional state of the trapped electron are feasible by microwave and optical means. Combined with the results studied in Ref. [13], the highly-efficient and high-fidelity quantum operations are available in the trapped-electron system, and this novel system manifests itself as a new playground for the development of quantum technologies.

We acknowledge Genya Watanabe, Shotaro Shirai and Yasunobu Nakamura for fruitful discussions. KT acknowledges SPRING GX and Q-step programs, and MS does WINGS-ABC program. This work is supported by JST ERATO MQM project (Grant No. JPM-JER1601), JSPS KAKENHI (Grant No. 19H01821) and JST SPRING (Grant No. JPMJSP2108).

-
- [1] C. D. Bruzewicz, J. Chiaverini, R. McConnell, and J. M. Sage, *Applied Physics Reviews* **6**, 021314 (2019).
- [2] M. Saffman, *J. Phys. B At. Mol. Opt. Phys.* **49**, 202001 (2016).
- [3] M. Kjaergaard, M. E. Schwartz, J. Braumüller, P. Krantz, J. I.-J. Wang, S. Gustavsson, and W. D. Oliver, *Annu. Rev. Condens. Matter Phys.* **11**, 369 (2020).
- [4] J. R. Weber, W. F. Koehl, J. B. Varley, A. Janotti, B. B. Buckley, C. G. V. de Walle, and D. D. Awschalom, *Proceedings of the National Academy of Sciences* **107**, 8513 (2010).
- [5] J. P. Gaebler, T. R. Tan, Y. Lin, Y. Wan, R. Bowler, A. C. Keith, S. Glancy, K. Coakley, E. Knill, D. Leibfried, and D. J. Wineland, *Phys. Rev. Lett.* **117**, 060505 (2016).
- [6] B. Foxen, C. Neill, A. Dunsworth, P. Roushan, B. Chiaro, A. Megrant, J. Kelly, Z. Chen, K. Satzinger, R. Barends, F. Arute, K. Arya, R. Babbush, D. Bacon, J. C. Bardin, S. Boixo, D. Buell, B. Burkett, Y. Chen, R. Collins, E. Farhi, A. Fowler, C. Gidney, M. Giustina, R. Graff, M. Harrigan, T. Huang, S. V. Isakov, E. Jeffrey, Z. Jiang, D. Kafri, K. Kechedzhi, P. Klimov, A. Korotkov, F. Kostritsa, D. Landhuis, E. Lucero, J. McClean, M. McEwen, X. Mi, M. Mohseni, J. Y. Mutus, O. Naaman, M. Neeley, M. Niu, A. Petukhov, C. Quintana, N. Rubin, D. Sank, V. Smelyanskiy, A. Vainsencher, T. C. White, Z. Yao, P. Yeh, A. Zalcman, H. Neven, J. M. Martinis, and Google AI Quantum, *Phys. Rev. Lett.* **125**, 120504 (2020).
- [7] A. Y. Kitaev, *Ann. Phys.* **303**, 2 (2003).
- [8] S. B. Bravyi and A. Yu. Kitaev, arXiv:quant-ph/9811052v1.
- [9] D. Wineland, P. Ekstrom, and H. Dehmelt, *Phys. Rev. Lett.* **31**, 1279 (1973).
- [10] N. Daniilidis, D. J. Gorman, L. Tian, and H. Häffner, *Quantum information processing with trapped electrons and superconducting electronics*, *New Journal of Physics* **15**, 073017 (2013).
- [11] S. Kotler, R. W. Simmonds, D. Leibfried, and D. J. Wineland, *Hybrid quantum systems with trapped charged particles*, *Phys. Rev. A* **95**, 022327 (2017).
- [12] C. Matthiesen, Q. Yu, J. Guo, A. M. Alonso, and H. Häffner, *Phys. Rev. X* **11**, 011019 (2021).
- [13] Q. Yu, A. M. Alonso, J. Caminiti, K. M. Beck, R. T. Sutherland, D. Leibfried, K. J. Rodriguez, M. Dhital, B. Hemmerling, and H. Häffner, *Phys. Rev. A* **105**, 022420 (2022).
- [14] T. Ruster, C. T. Schmiegelow, H. Kaufmann, C. Warschburger, F. Schmidt-Kaler, and U. G. Poschinger, *Appl. Phys. B* **122**, 254 (2016).
- [15] A. M. J. Zwerver, T. Krähenmann, T. F. Watson, L. Lampert, H. C. George, R. Pillarisetty, S. A. Bojarski, P. Amin, S. V. Amitonov, J. M. Boter, R. Caudillo, D. Corras-Serrano, J. P. Dehollain, G. Droulers, E. M. Henry, R. Kotlyar, M. Lodari, F. Lüthi, D. J. Michalak, B. K. Mueller, S. Neyens, J. Roberts, N. Samkharadze,

- G. Zheng, O. K. Zietz, G. Scappucci, M. Veldhorst, L. M. K. Vandersypen, and J. S. Clarke, *Nature Electronics* **5**, 184 (2022).
- [16] K. Mølmer and A. Sørensen, *Phys. Rev. Lett.* **82**, 1835 (1999).
- [17] P. Peng, C. Matthiesen, and H. Häffner, *Phys. Rev. A* **95**, 012312 (2017).
- [18] W. M. Itano, J. C. Bergquist, J. J. Bollinger, and D. J. Wineland, *Cooling methods in ion traps*, *Physica Scripta* **T59**, 106 (1995).
- [19] H. J. Kimble, *Nature* **453**, 1023 (2008).
- [20] S. M. Brewer, J.-S. Chen, A. M. Hankin, E. R. Clements, C. W. Chou, D. J. Wineland, D. B. Hume, and D. R. Leibbrandt, *Phys. Rev. Lett.* **123**, 033201 (2019).
- [21] P. Reinhold, S. Rosenblum, W.-L. Ma, L. Frunzio, L. Jiang, and R. J. Schoelkopf, *Nature Physics* **16**, 822 (2020).
- [22] T. Dubielzig, S. Halama, H. Hahn, G. Zarantonello, M. Niemann, A. Bautista-Salvador, and C. Ospelkaus, *Rev. Sci. Instrum.* **92**, 043201 (2021).
- [23] G. Vrijsen, Y. Aikyo, R. F. Spivey, I. V. Inlek, and J. Kim, *Opt. Express* **27**, 33907 (2019).
- [24] H. Shao, M. Wang, M. Zeng, H. Guan, and K. Gao, *J. Phys. Commun.* **2**, 095019 (2018).
- [25] A. Osada and A. Noguchi, *J. Phys. Commun.* **6**, 015007 (2022).
- [26] S. Gulde, D. Rotter, P. Barton, F. Schmidt-Kaler, R. Blatt, and W. Hogervorst, *Appl. Phys. B* **73**, 861 (2001).
- [27] A. Wallraff, D. I. Schuster, A. Blais, L. Frunzio, R.-S. Huang, J. Majer, S. Kumar, S. M. Girvin, and R. J. Schoelkopf, *Nature* **431**, 162 (2004).
- [28] J. R. Schrieffer and P. A. Wolff, (1966).
- [29] D. I. Schuster, A. A. Houck, J. A. Schreier, A. Wallraff, J. M. Gambetta, A. Blais, L. Frunzio, J. Majer, B. Johnson, M. H. Devoret, S. M. Girvin, and R. J. Schoelkopf, *Nature* **445**, 515 (2007).
- [30] M. F. Gely, M. Kounalakis, C. Dickel, J. Dalle, R. Vatré, B. Baker, M. D. Jenkins, and G. A. Steele, *Science* **363**, 1072 (2019).
- [31] N. Leefer, K. Krimmel, W. Bertsche, D. Budker, J. Fajans, R. Folman, H. Häffner, and F. Schmidt-Kaler, *Hyperfine Interact.* **238**, 12 (2016).
- [32] H. Dehmelt, *Phys. Scr.* **1995**, 423 (1995).
- [33] C. J. Foot, D. Trypogeorgos, E. Bentine, A. Gardner, and M. Keller, *Int. J. Mass Spectrom.* **430**, 117 (2018).
- [34] D. R. Leibbrandt, J. Labaziewicz, R. J. Clark, I. L. Chuang, R. J. Epstein, C. Ospelkaus, J. H. Wesenberg, J. J. Bollinger, D. Leibfried, D. J. Wineland, D. Stick, J. Sterk, C. Monroe, C.-S. Pai, Y. Low, R. Frahm, and R. E. Slusher, *Quantum Inf. Comput.* **9**, 901 (2009).
- [35] A. Noguchi, R. Yamazaki, Y. Tabuchi, and Y. Nakamura, *Nat. Commun.* **11**, 1183 (2020).
- [36] M. Aspelmeyer, T. J. Kippenberg, and F. Marquardt, *Rev. Mod. Phys.* **86**, 1391 (2014).
- [37] D. R. Leibbrandt, R. J. Clark, J. Labaziewicz, P. Antohi, W. Bakr, K. R. Brown, and I. L. Chuang, *Phys. Rev. A* **76**, 055403 (2007).

Appendix A: Calcium titanate as a long-lived ablation target

As stated in Sec. IIB, pulsed laser ablation is relevant for loading ions and electrons into the Paul trap, however, the lifetime of the ablation target is crucial for the vacuum-sealed experiment running for months long. The lifetime, or how many ablation pulses the target can endure, can vary over target materials [37] and we here investigate such property of metallic calcium and ceramic calcium titanate as target materials and compare the results.

The 1064 nm-wavelength, nanosecond pulsed laser with pulse fluence of 3 J/cm² is shoot on the samples and the fluorescence of the calcium atoms can be observed when 423 nm-wavelength laser path crosses the atom jet. Figure 6 shows the observed fluorescence counts as the number of the applied ablations pulsed at the same target point increases. As can be seen in the plots, the signal for the calcium titanate (red) persists for thousands of ablation pulses in contrast to the metallic calcium (gray), meaning that the calcium titanate is a better target ma-

terial than metallic calcium.

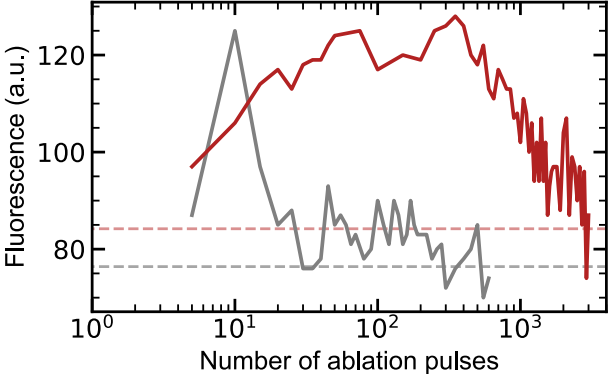
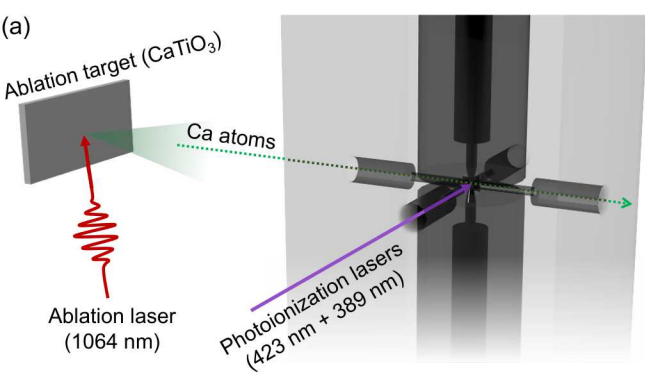


FIG. 6. Fluorescence counts as a function of the number of ablation pulses. Red (gray) plot is for the calcium titanate (metallic calcium) with the background noise level indicated by a red (gray) broken line.



(b)